Geotextiles and Geomembranes 28 (2010) 44–53

Contents lists available at ScienceDirect

Geotextiles and Geomembranes

journal homepage: www.elsevier.com/locate/geotexmem

Physical and analytical modelling of geosynthetic strip pull-out behaviour

Abdelkader Abdelouhab [a,*], Daniel Dias [a], Nicolas Freitag [b]

[a] Inst. Nat. Sc. Appl. Lyon, Laboratory of Civil and Environmental Engineering LGCIE, 20 av. A. Einstein, F 69621 Villeurbanne Cedex, France
[b] Research & Development Manager, Terre Armée internationale, 1 bis, rue du Petit-Clamart, 78140 Vélizy-Villacoublay, France

ARTICLE INFO

Article history:
Received 12 January 2009
Received in revised form
2 August 2009
Accepted 23 September 2009
Available online 29 October 2009

Keywords:
Mechanically stabilised earth (MSE) structures
Geosynthetic reinforcements
Soil/structure interaction
Pull-out tests
Analytical modelling

ABSTRACT

The design methods used for soil mass structures, such as mechanically stabilised earth (MSE) structures, are based on soil/reinforcement anchorage models which require the knowledge of the soil/reinforcement interface friction capacity. However, different types of reinforcements are used in these structures and present different behaviour. This study concerns two types of strips reinforcements. The first one is metallic and is classically designed using elasto-plastic models (Schlosser and Guilloux 1981, Segrestin and Bastick 1996). The second type is geosynthetic. The classical anchorage models do not take into account the extensibility of this materiel and do not reproduce its complex behaviour.

In the first part this paper presents pull-out tests carried out on the two types of strips reinforcements (metallic and synthetic) subjected to several levels of vertical stresses. The tests are carried out in a metallic tank in controlled and instrumented conditions. In the second part, three modelling processes of the pull-out tests are implemented. The first method takes classical anchorage models into account. The second method improves the friction model using the analysis of the experimental tests. The last method adds the real tensile behaviour of the synthetic reinforcement to the second and assumes an initial strain threshold ε_0 (Bourdeau et al. 1990) in order to simulate the delayed mobilisation. This analysis leads to parameters which qualify the interaction between metallic or synthetic strips and the soil mass, and enable a better understanding of the behaviour of the structures.

1. Introduction

In mechanically stabilised earth (MSE) structures, a granular soil mass is set up in successive horizontal layers between reinforcing elements (metallic or synthetic strips). Generally, ribbed steel strips are used in these types of structures. However, in aggressive environments, geosynthetic straps are preferred due to their non-corrodible properties.

Currently, the methods used for the modelling of this structure type are based on the classical anchorage models of reinforcement (linear strip stiffness model for the reinforcement and an elasto-plastic friction model for the interface). These methods, developed for the metallic, and thus inextensible, reinforcements, were simply extrapolated to extensible materials. This practice is justified only if structure stability has to be ensured. But the deformation behaviour is more complex, thus the use of new models is necessary for a better optimisation of these structures.

These last years, many experimental tests (Yoo and Kim 2008, Won and Kim 2007) and theoretical studies (Leshchinsky 2009, Ling et al., 2005, Koerner and Soong, 2001, Yoo and Jung 2006) have been carried out on geosynthetic reinforced soil walls. However, most of them focus on the global stability of these structures.

In order to take into account the real behaviour of the structures reinforced by extensible reinforcement, it is necessary to have information on:

- the reinforcement material: a tensile test on a free synthetic strap gives the definition of its characteristics;
- the soil/reinforcement interaction: the force that develops in the strap is a tensile stress which results from the shear stress between the reinforcement and the soil. The deformations of the soil and the inclusion have an important influence on the shear stress distribution along the reinforcement. Thus, the interface friction cannot be considered as a local phenomenon (Schlosser and Guilloux, 1981). A pull-out test allows us to simulate the tensile stress applied on the reinforcement and to define the evolution of the interface parameters during its mobilisation (Sieira et al., 2009, Khedkar and Mandal, 2009, Su et al., 2008, Palmeira, 2009). Unlike the direct shear test, the pull-out test highlights the evolution of several parameters: shear stress and friction along the soil/reinforcement interface;

* Corresponding author.
E-mail addresses: abdelkader.abdelouhab@insa-lyon.fr (A. Abdelouhab), daniel.dias@insa-lyon.fr (D. Dias), nfreitag@terre-armee.com (N. Freitag).

0266-1144/$ – see front matter © 2009 Elsevier Ltd. All rights reserved.
doi:10.1016/j.geotexmem.2009.09.018

Nomenclature

HA	high adherence
J	geosynthetic elongation modulus (kN/m)
L	reinforcement length (m)
T	tensile force (kN)
T_H	tensile force at the head of the reinforcement (kN)
$T_{(x)}$	tensile force along reinforcement (kN)
U^*	relative soil/reinforcement displacement corresponding to the total mobilisation of friction (mm)
U_H	head displacement (mm)
U_R	rear displacement (mm)
$U_{(x)}$	displacement along reinforcement (mm)
b	reinforcement width (m)
dx	infinitesimal element length along soil-reinforcement interface (m)
f	friction coefficient at the soil/reinforcement interface
f^*	maximum apparent friction coefficient at the soil/reinforcement interface
K_0	coefficient of earth pressure at rest
σ_v	initial vertical stress applied on the reinforcement (kPa)
φ	friction angle (°)
γ	bulk unit weight (kN/m^3)
τ	interface shear stress (kPa)
τ^*	maximum interface shear stress (kPa)
ε	local strain
ε_0	initial strain threshold

the soil dilatancy and the reinforcement strain. These parameters are taken into account in several design methods of MSE walls (e.g. Norme française NF P 94–270, 2009).
- the granular soil mass: classical tests define its geotechnical parameters.

Considering the real behaviour of the constitutive material as well as parameters governing the behaviour of the soil/synthetic reinforcement interface by experimental tests, more realistic anchorage models are determined.

The classical anchorage models are based on a linear strip stiffness model for the reinforcement and an elasto-plastic friction model (Cambefort, 1964, Frank and Zhao, 1982) for the soil/reinforcement interaction. These assumptions are not accurate enough when considering the behaviour of the synthetic reinforcement.

Several anchorage models were previously proposed. Some authors make an improvement of the stiffness model for the reinforcement materiel:

- Bourdeau et al. (1990) presents a modified stiffness model which admits an ε_0 at the beginning corresponding to an initial strip strain before there is any tensile-load application. It takes into account the elongation of flexible inclusions.
- Ling et al. (1992) formulate the geosynthetic elongation modulus as a nonlinear function of the confinement stress level. Indeed, Wu (1991) and Ballegeer and Wu, (1993) obtain different values of the elongation modulus for geosynthetic reinforcements according to the confinement conditions.

Other authors take into account the interaction parameters at the soil/reinforcement interface:

- Sobhi and Wu (1996) suggest an analytical model supposing that each segment of the reinforcement passes through three states, a stationary state of confinement, a state of friction mobilisation at the soil/reinforcement interface and, finally, a state of cumulative strain. Based on the experimental results, they propose methods to predict the state of each zone of the reinforcement at the time of the head tensile-load application.
- Gurung et al. (1999) express the results of tensile-load-displacement along an extensible reinforcement subjected to the pull-out, in the form of a differential equation of a nonlinear hyperbolic behaviour. The modelling results are rather close to the laboratory test results carried out by Sobhi and Wu (1996) and Abramento and Whittle (1995).
- Racana et al. (2003) show that the tensile load applied along a flexible reinforcement anchored in the ground, is not homogeneous. Because of its flexibility, the reinforcement presents corrugated zones where the tensile load is lower than the straight zones. So, they suggest taking into account, in practice, a shorter reinforcement length than reality to approach the real conditions.

In this paper we present two new models. The first takes into account a realistic friction model at the soil-reinforcement interface with a simple strip stiffness model. The second adds a real strip stiffness model to the previous one. Then they are confronted with a classical modelling method. These new models are validated and their parameters are generalised after application on all the pull-out tests carried out in laboratory.

2. Three-dimensional physical modelling

Pull-out tests were carried out on metallic and synthetic reinforcements in a granular material. The material used in the tests is fine sand known under the name of Hostun RF sand. Various authors have studied this material (Gay 2000, Flavigny et al., 1990). The main physical and granulometric characteristics are referred to on Table 1.

Two reinforcement types have been used: metallic and geosynthetic. Commonly, in MSE walls, only one metallic strip is connected to each attachment point of the facing panel. For the walls reinforced by synthetic reinforcement, one pair of parallel straps, 50 mm apart, is connected to each attachment point of the facing panel. The influence of the close synthetic straps could lead to a different behaviour.

For the metallic reinforcements, only one metallic strip is pulled out in each test. For the synthetic reinforcements, two types of test were carried out:

- The pulling-out of only one strap. This installation enables us to compare the results obtained between one metallic and one synthetic strap.
- The pulling-out of pair of parallel synthetic straps. This layout reproduces conditions closer to real structures.

Table 1
Characteristics of the Hostun RF sand

Characteristics	Value	Characteristics	Value
Granulometry (mm)	0.16–0.63	Angle of friction (°)	38
D10 (mm)	0.2	Dilatancy (°)	8
D60 (mm)	0.42	Unit weight of the grains (kN/m3)	26.5
Maximum index of vacuums	1.041	Maximum volumic weight (kN/m3)	15.99
Minimal index of vacuums	0.648	Minimal volumic weight (kN/m3)	13.24

2.1. Procedure

The tests were carried out in the following way: half of a metallic tank is filled by pluviation with a granular material. Reinforcement (synthetic or metallic) is installed on the flat surface of the sand and connected to an extraction jack positioned in front of the tank. Three types of connection systems were conceived in order to carry out the tests on: only one synthetic strap; two parallel synthetic straps and one metallic strip. Displacement sensors installed at the back of the tank, are connected to various points along the reinforcement to measure displacements. A load sensor installed between the extraction jack and the connection system enables the measurement of the tensile force applied at the head during the test. After connecting all the sensors, the tank is finally filled with granular material. An air cushion, which permits the application of a surcharge, is then placed between the ground inside the tank and the tank closure. This cushion is inflated by air pressure and controlled by a pressure gauge. Before installing the air cushion metallic plates are placed on the ground surface. These rigid plates permit a better simulation of the boundary limits of a soil layer inside a segmental reinforced retaining wall. Lastly, after closing the tank and applying the pressure in the air cushion, one starts the extraction jack. The pressure in the cushion is kept constant during the pull-out test. Within the framework of our tests, the pull-out speed is fixed at 1 mm/min, corresponding to a value commonly adopted (Alfaro et al., 1995).

2.2. Description of tools and materials

2.2.1. Reinforcements

- Geosynthetic

The synthetic reinforcements used in the tests are straps which are 50 mm wide and 2 mm thick containing high-tenacity polyester yarns protected by a polyethylene sheath (Fig. 1a). Known under the name of GeoStraps, they are used in Reinforced Earth structures without any metal (thus corrodible) intermediary.

- Metallic

The steel strip is made of galvanised and ribbed steel and known under the name of High Adherence strip (HA 50 x 4). In this case, the dimensions are: width: 50 mm and thickness: 4 mm (Fig. 1b).

2.2.2. The experimental tank

The pull-out tests were carried out with an experimental device which conforms to the standards recommendations ASTM D6706-01 and EN 00189016. The test tank is metallic with large inner dimensions: 1.10 m wide, 1.10 m high and 2.0 m long

The position of the synthetic straps in the tank and the measuring points on the straps are illustrated in Fig. 2 which shows how the reinforcement is fixed to the connection system for the tests carried out on two synthetics straps. Two other connection systems were used to connect the metallic strip and one synthetic strap to the extraction jack.

The measuring points enable us to monitor the displacement of each part of the strap and to highlight the progressive mobilisation of the reinforcement.

2.2.3. The sensors

- Displacement sensors

To measure displacements along and at the head of the reinforcement, cable displacement sensors with a capacity of 250 mm are used. They are placed on the support at the front and the back of the tank then lengthened and connected by a steel cable of 1 mm diameter at various points on the reinforcement. In order to avoid any friction effect with the soil, these cables are sheathed in Teflon.

- Load sensor

In order to measure the tensile force, a load sensor is placed between the extraction jack and the connection system.

3. Analysis of experimental results

3.1. Tests carried out

Altogether, 26 tests were carried out. 5 tests on the metallic reinforcement, 8 tests on only one synthetic strap and 13 tests on two parallel synthetic straps. These tests enabled us to compare and better understand the behaviour of the two types of reinforcement (synthetic and metallic) and to evaluate the difference between the set up of one or two parallel straps.

Five levels of confinement stress were applied in tests (7 kPa, 22 kPa, 40 kPa, 60 kPa and 80 kPa) to simulate various depth levels of a real structure. The ground density values obtained in all the tests are very close and vary between 1.51 and 1.54. It shows that the pluviation system can reproduce a required ground density.

3.2. Results analysis

3.2.1. Stresses distribution in the test tank

Pull-out test results can be influenced by boundary conditions. In this physical model, a pressure is applied on the surface of the tank. Due to friction on the internal tank walls, some uncertainties on vertical stress at the reinforcement level can remain. Commonly,

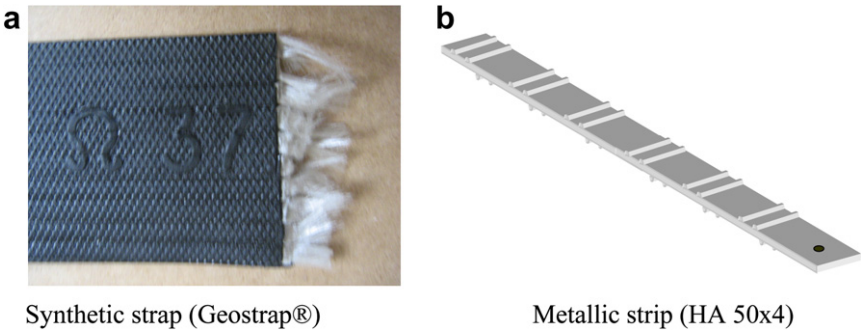

Fig. 1. Reinforcement: a. Synthetic strap (Geostrap®) b. Metallic strip (HA 50x4).

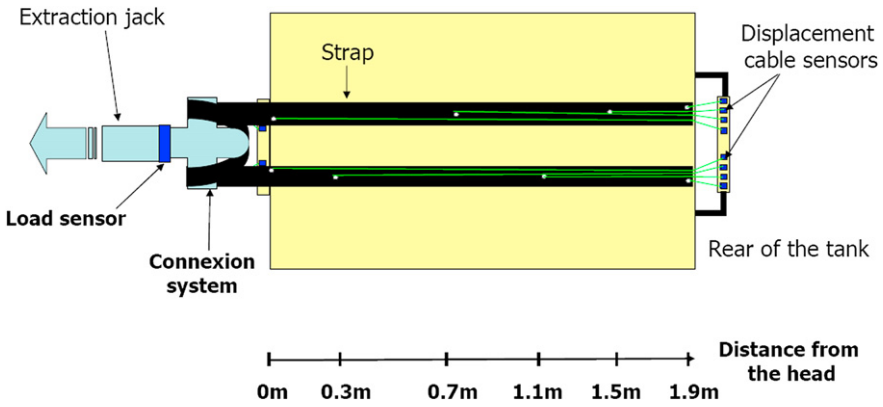

Fig. 2. Position of two parallel synthetic straps and the displacement sensors.

to avoid this problem, a double layer of polythene is laid between the soil and the tank walls with grease or oil between the two polythene layers (Palmeira and Milligan, 1989). This technique is time consuming during the installation. In our case, the set up of load sensors at the bottom and on the tank walls has been chosen in order to control the stresses distribution. The results obtained by these load sensors show that the stresses measured at the bottom are lower by 30–40% than those applied on the surface.

To determine the stresses applied at the tank centre, where the reinforcement is anchored, load sensor results and analytical calculation using Terzaghi's formula are combined (See Appendix A). First, the results obtained from the analytical method at the bottom of the tank are validated by the sensors measurement. Then the stresses applied at the center of the tank are calculated by the analytical method.

3.2.2. *Influence of the confinement stress*

- On the reinforcement mobilisation

The mobilisation along the metallic reinforcement is instantaneous for any confinement stress. However, the synthetic strap behaviour is more complex and varies with the confinement stress variation. Fig. 3 shows that in the case of the synthetic strap, for a confinement stress of 7 kPa, the curve of the tensile stress versus the displacement can be assimilated to a bilinear model. For a confinement stress of 80 kPa, the curve is close to a three-linear model. The defining of a new friction model will be based on the parameters of these curves.

The analysis of the head displacement versus the rear displacement of the two reinforcement types (Fig. 4) shows that the mobilisation along the metallic reinforcement is instantaneous. The rear moves when the head moves. On the other hand, in the case of the synthetic reinforcement, a delay can be observed. Tension, as well as displacements, is gradually mobilised from the head to the rear of the straps. So, the tail is mobilised after the displacement threshold at the head is reached. This threshold increases as the confinement stress increases. The mobilised length of the reinforcement depends on the head displacements and on the confinement stress. The mobilised length of the strap increases as displacement at the head is increased.

- On the soil/reinforcement interface friction

In a dense and dilatant granular soil, under the effect of shear stresses τ exerted by reinforcements, the volume of the surrounding zone tends to increase (Schlosser and Elias, 1978; Schlosser and Guilloux, 1981). This results in an increase ($\Delta\sigma_v$) of the initial vertical stress σ_{v0}. Hence, the vertical stress σ_v applied on the inclusion becomes $\sigma_v = \sigma_{v0} + \Delta\sigma_v$. This phenomenon is named constrained dilatancy. The real friction coefficient f is thus expressed:

$$f = \frac{\tau_{max}}{\sigma_{v0} + \Delta\sigma_v}$$

The three-dimensional character of this phenomenon and the influence of dilatancy are difficult to take into account in design methods. Schlosser and Elias, 1978, defined an apparent friction coefficient f^* to take this phenomenon into account in practice:

$$f^* = \frac{\tau_{max}}{\sigma_{v0}}$$

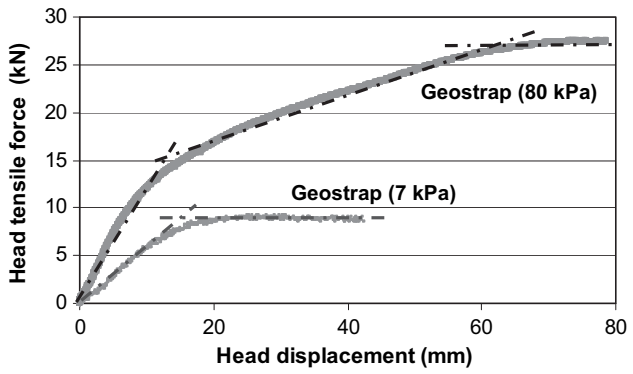

Fig. 3. Behaviour at the head of synthetic reinforcement under two different confinement stresses.

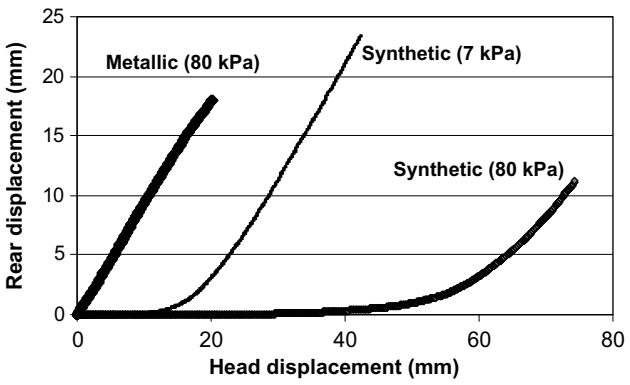

Fig. 4. Rear displacement versus head displacement of metallic and synthetic reinforcement under two different confinement stresses.

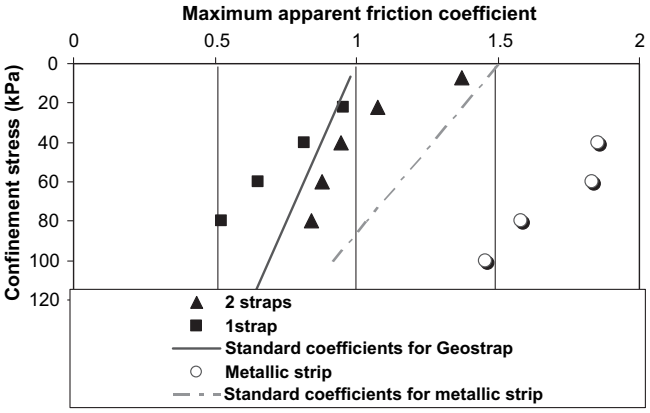

Fig. 5. Variation of apparent friction coefficient versus confinement stress for the synthetic and metallic reinforcements.

Fig. 5 shows that the maximum friction coefficient at the soil/reinforcement interface decreases as the confinement stress increases on the two types of reinforcement (metallic and synthetic) and also for the two layout types of the synthetic reinforcement (one and two parallel straps) due to the constrained dilatancy phenomenon.

3.2.3. Influence of the layout of the synthetic straps

The confrontation of the values of the maximum friction coefficient, between two straps and one strap, shows that this parameter is greater in the case of two straps, especially under high confinement stresses (Fig. 5). Therefore, two parallel, closely spaced synthetic straps improve the friction between the ground and the reinforcement under high confinement stresses. It permits us to obtain better friction coefficients than those used in practice in the design of MSE walls. This friction improvement is probably related to an arching effect and a soil dilatancy which are created between the two straps and thus increases the stress area around the inclusions (Fig. 6).

4. Analytical and numerical modelling

Modelling reinforcements anchored in a soil mass and subjected to a tensile force, requires the knowledge of two models:

- the reinforcement stiffness model $T - \varepsilon$(Fig. 7); this defines the relation between the applied tensile force (T) and the strain using the elongation modulus ($J = \mathrm{ES}$).

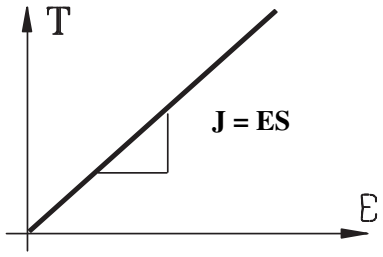

Fig. 7. Strip stiffness model.

- a local friction model ($f - U$) between the ground and the reinforcement (Fig. 8); this defines the relation between the soil/reinforcement friction (f) and the relative displacement (U). The parameters of this model are the maximum friction coefficient (f^*) and the equivalent displacement (U^*).

Usually, the shear stress (τ) is used in the expression of the friction model. However, to take into account the ground dilatancy, the apparent friction coefficient (f^*) is used.

Three modelling approaches sorted by increasing order of complexity were implemented. The first modelling M1, considers simple behaviours for the two models (friction and stiffness model), the second M2, takes into account a more realistic friction model and finally, the third M3, uses the real behaviour of the synthetic straps. In this study, only the first was used for the metallic reinforcements.

4.1. First modelling (M1)

In this case, the method adopted by Schlosser and Guilloux, (1981), Segrestin and Bastick (1996) was implemented. The shear stress (τ) is replaced by the apparent friction coefficient ($f = \tau/\sigma_v$) (Fig. 8). The strip stiffness model is a classical model ($T = J\varepsilon$).

The principle of the method M1 consists in writing the equilibrium of forces in each infinitesimal strap section by combining the elasto-plastic strip stiffness model with the classical local friction model. Differential equations are obtained and solved analytically considering three mobilisation stages of the strap (see Appendix B). The solution of the equation makes it possible at each stage to calculate tensile force and displacements at each point x along the reinforcement.

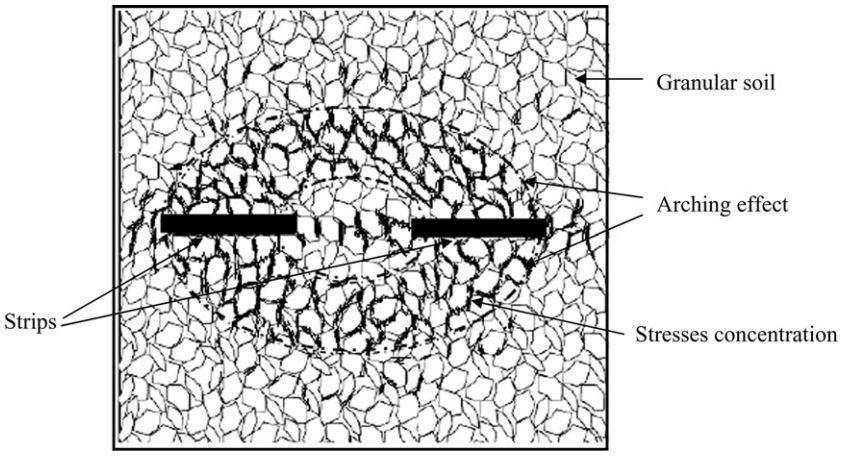

Fig. 6. Schematisation of the arching effect around the reinforcement.

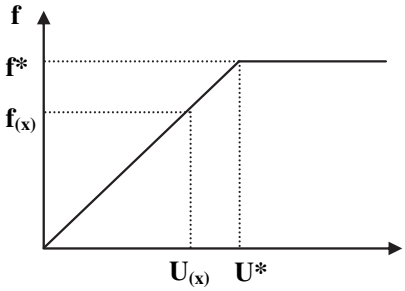

Fig. 8. Local friction model.

4.2. Second modelling (M2)

The curves analysis $T_H = f(U_H)$ obtained from the pull-out tests led to a square root model for the soil/reinforcement interface friction (Fig. 9). The strip stiffness model of M1 is preserved. Thus, the local friction model taken into account is defined in the following way:

$$f(x) = f^* \sqrt{U/U^*}$$

Combining the square root friction model with the elasto-plastic strip stiffness model leads to more complex differential equations which are non-solvable by analytical development. A discretisation of the square root curve was thus carried out and led to classical differential equations. These equations are numerically solved by using Matlab. Fig. 9 shows an example of this process, for $U < U^*_{final}$ the root curve is divided into n phases which lead to n differential equations. In each of these phases, we consider a simple elastic model as in the first modelling M1.

When considering U^*_{i-1} and f^*_{i-1} as the origin of the curve in each step i (Fig. 9), we deduce: $U(x)/U^*_i = f(x)/f^*_i$. Combining this relation with the equation (1) (see Appendix B):

$$dT(x) = 2bf(x)\sigma_v dx \quad (1)$$

we obtain:

$$\frac{dT(x)}{dx} = 2bf^*_i \sigma_v \frac{U(x)}{U^*_i} \quad (2)$$

The local strain $\varepsilon_{(x)}$ at the point of abscissa x is given by the strip stiffness model (see Appendix B).

$$\frac{dU(x)}{dx} = \frac{T(x)}{J} = \varepsilon(x) \quad (3)$$

From (2) and (3):

$$\frac{d^2U(x)}{d^2x} - \frac{2bf^*_i \sigma_v}{JU^*_i} U(x) = 0 \text{ and } \frac{d^2T(x)}{d^2x} - \frac{2bf^*_i \sigma_v}{JU^*_i} T(x) = 0 \quad \text{if } U \le U^*_{final}$$

$$\frac{d^2U(x)}{d^2x} - \frac{2bf^*_i \sigma_v}{J} = 0 \text{ and } \frac{dT(x)}{dx} - 2bf^*_i \sigma_v = 0 \quad \text{if } U > U^*_{final}$$

The numerical solution of these equations allows the calculation of the tensile force and displacement at each point x of the reinforcement.

4.3. Third modelling (M3)

The strip stiffness model was also improved in order to better take into account the delayed mobilisation of the synthetic reinforcements. This was done by taking into account the real strip stiffness model, using results from tensile tests carried out on a free synthetic strap. A complement was added to this model by introducing an initial strain ε_0 (Bourdeau et al., 1990). Indeed, in real conditions, due to the flexibility of the reinforcement and of the non-uniformity of the surface on which it is installed, an initial strain ε_0 is reached without even applying a tensile force (Fig. 10).

The strip stiffness models determined by tensile tests for one and two synthetic straps are taken as nonlinear curves approximated by polynomial functions ($T = a_0 + a_1\,\varepsilon + a_2\,\varepsilon^2 + a_3\,\varepsilon^3 + a_4\,\varepsilon^4 + a_5\,\varepsilon^5 + a_6\,\varepsilon^6 + a_7\,\varepsilon^7 + a_8\,\varepsilon^8$). It permits the accurate reproduction of the strip behaviour for a stiffness of the strip $\varepsilon \le 11.5\%$. The values of the polynomial function coefficients for one and two synthetic straps are specified in Table 2.

The new strip stiffness model becomes $T(x) = \sum a_i \varepsilon^i(x)$, which leads to:

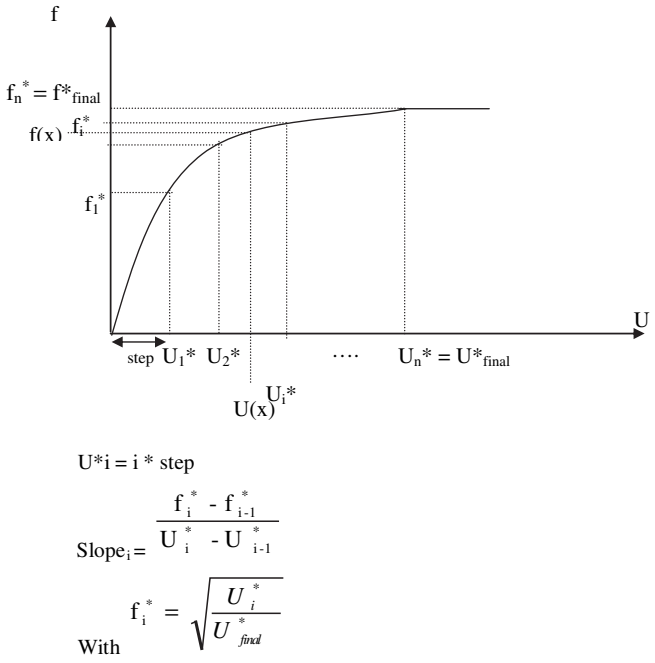

Fig. 9. Square root friction model divided into n phases.

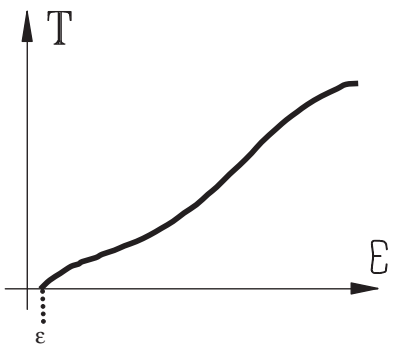

Fig. 10. Modified synthetic strap stiffness model ($\varepsilon = T/J + \varepsilon_0$).

$$\frac{dT(x)}{dx} = \sum i a_i \varepsilon^{i-1}(X)\frac{d\varepsilon(x)}{dx}$$

The introducing of ε_0 leads to:

$$T(X) = \sum a_i(\varepsilon(X) - \varepsilon_0)^i \text{ and } \varepsilon(X) = \sum b_i T(X)^i + \varepsilon_0$$

Combining this new model with the discretised square root friction model led to differential equations. Solving these equations numerically enabled the calculation of the tensile force and displacement at each point x of the reinforcement.

4.4. Search for optimum parameters for the three modelling approaches

Analysis using the three previous modelling approaches induces an optimisation of the parameters allowing us to simulate the experimental tests with the highest degree of accuracy. These parameters are specified in Table 3. An automatic optimisation was implemented with Matlab software. The criterion used to estimate the error between the modelling result and the experimental result is as follows:

$$E = \sqrt{\sum (u_{i\ \text{calculated}} - u_{i\ \text{measured}})^2}$$

The parameters retained for the anchorage models are those which lead to the smallest error.

4.5. The efficiency of modelling approaches

Using experimental tests, the parameters for the three modeling approaches were calculated using the optimisation approach.

In the case of the metallic strip, only the first method M1 was used. It leads to the correct reproduction of the strip behaviour at the head (Fig. 11).

Fig. 12 shows the comparison between the experimental tests on the synthetic straps and the modelling method M3 for a confinement stress of 80 kPa. The three modelling approaches reproduce the head displacements well. The theoretical and experimental results almost follow the same curve, in particular in the case of one strap.

For the rear displacement, M1 considers that the reinforcement is instantaneously mobilised along its entire length. In the case of the metallic strip, it gives good results and reproduces the end displacement of the strip well (Fig. 13). For the synthetic straps, this method leads to a discrepancy between the experimental and the theoretical curves (Fig. 14). M2 gives better results than M1 and allows us to simulate a small delay of mobilisation at the strap end. However, a discrepancy between the theoretical and the experimental curves is still observed in this modelling. M3 led to a better simulation of the mobilisation of the synthetic straps. Indeed, as shown in Fig. 14, the curves of the end strap displacement obtained from this method are almost perfectly superimposed on the experimental curves.

Table 2
Parameters of the strip stiffness models.

Parameter	1 Synthetic strap	2 Synthetic straps
a_0	4.75×10^{-4}	4.76×10^{-4}
a_1	-2.80×10^{-5}	-1.48×10^{-5}
a_2	2.36×10^{-4}	5.92×10^{-5}
a_3	1.50×10^{-4}	1.88×10^{-5}
a_4	-2.72×10^{-5}	-1.70×10^{-6}
a_5	1.96×10^{-6}	6.11×10^{-8}
a_6	-7.15×10^{-8}	-1.12×10^{-9}
a_7	1.32×10^{-9}	1.03×10^{-11}
a_8	-9.73×10^{-12}	-3.80×10^{-14}

Table 3
Necessary inputs to modelling.

Experimentally determined parameters	f^*, J
Optimisationally determined parameters	U^*, ε_0

Modelling results obtained on one strap are slightly better than those of the two straps (Table 4). The arching phenomenon between two straps and its influence on the straps behaviour is not taken into account in the modelling.

The error displacement values calculated at the strap end for the 3 modelling methods (Table 4), confirms that the modelling M1 is

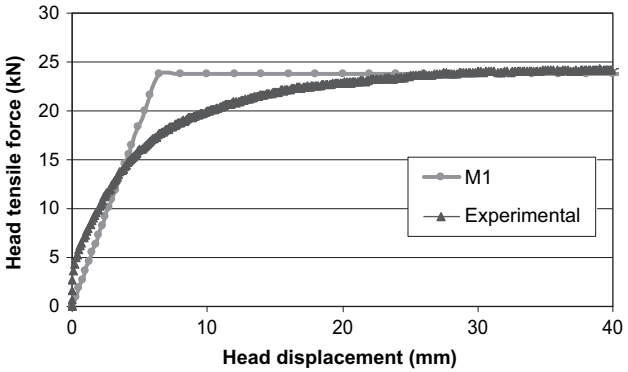

Fig. 11. Confrontation of the experimental and modelling results (strip head – metallic strip - confinement stress = 80 kPa).

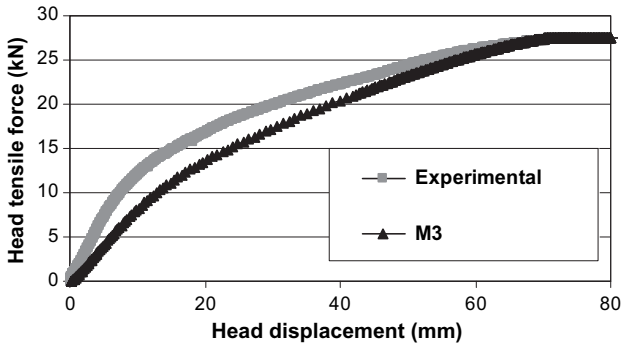

Fig. 12. Confrontation of the experimental and modelling results (strap head – two synthetic straps – confinement stress = 80 kPa).

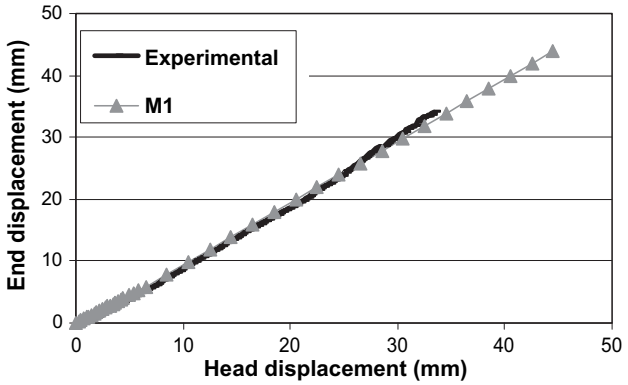

Fig. 13. Confrontation of the experimental and modelling results (strip end – metallic strip – confinement stress = 80 kPa).

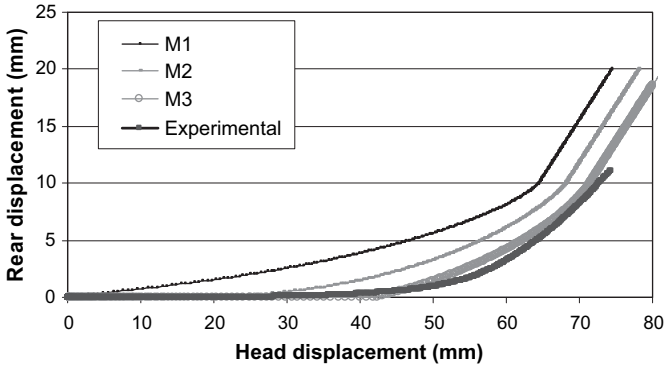

Fig. 14. Confrontation of the experimental and modelling results (strap end – two straps – confinement stress = 80 kPa).

adapted only to the metallic reinforcement and the modelling M3 leads to a better simulation of the synthetic strap behaviour.

4.6. Generalisation of modelling parameters

The modelling of all tests allowed us to validate the third modelling (M3) and led to the determination of the soil-structure interaction parameters. A generalisation of these parameters was realised after the modelling of all the tests.

4.6.1. Relative soil/reinforcement displacement corresponding to total mobilisation of friction (U^*)

The evolution of the parameter U^* versus the confinement stress is represented by three different curves (Fig. 15). The first one represents the evolution of these parameters in the case of the modelling of only one synthetic strap, the second one represents the modelling of two synthetic straps and the third one represents the modelling of the metallic strip. These curves are approximated by the following linear equation:

$$U^* = \alpha\sigma_v + \beta$$

Table 4
. Error function at the end of the reinforcement.

Type of strip	Confinement	22 (kPa)		40 (kPa)		80 (kPa)	
		1 Strap	2 Straps	1 Strap	2 Straps	1 Strap	2 Straps
Metallic	Modelling 1	–	–	4	–	3	–
Synthetic	Modelling 1	68	77	15	57	16	66
	Modelling 2	68	76	15	55	12	59
	Modelling 3	8	9	8	51	5	15

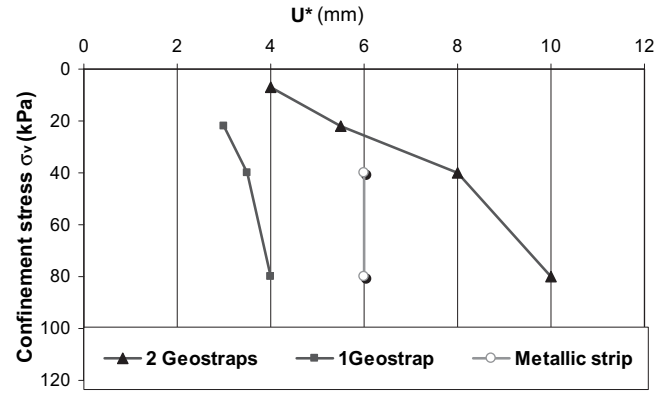

Fig. 15. U^* evolution versus confinement stress.

Table 5
Friction model parameters.

	1 Synthetic strap	2 Synthetic straps	Metallic strip
α (mm/kPa)	0.017	0.09	0
β (mm)	2.7	3.7	6

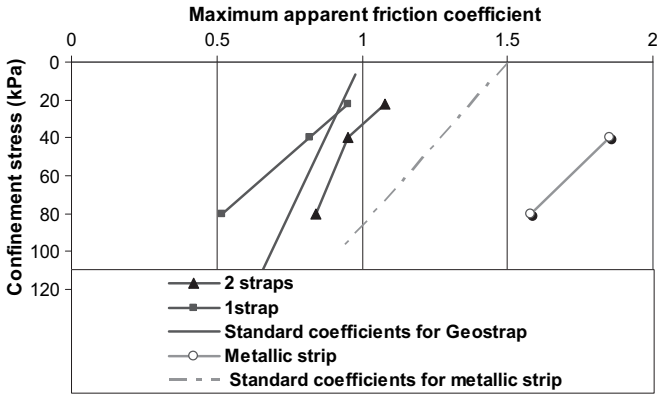

Fig. 16. f^* evolution versus confinement stress.

The values of α and β are specified in Table 5 for different cases (one synthetic strap, two synthetic straps and one metallic strip); $\sigma_v$is the confinement stress (kPa).

4.6.2. Maximum friction coefficient at the soil/reinforcement interface (f^*)

The evolution of f^* versus the confinement stress is presented in Fig. 16. These three curves are rather close to the standard line used in the internal design of the MSE walls. The equation of this standard line is:

$$f^* = f_0^* \times \frac{(120 - \sigma_v)}{120} + f_1^* \frac{\sigma_v}{120}$$

with f_0^*as the maximum friction coefficient at the top surface of the retaining walls (where $\sigma_v = 0$) and f_1^* is the maximum friction coefficient at a depth of 6 m (where $\sigma_v = 120$ kPa) in the retaining wall (NF P 94-220-0).

σ_v is the confinement stress expressed in kPa.

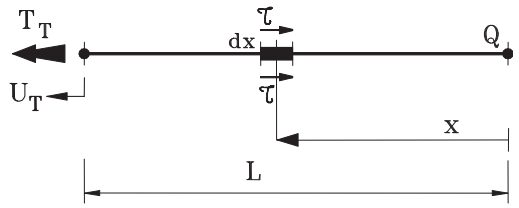

Fig. 17. Strip modelling.

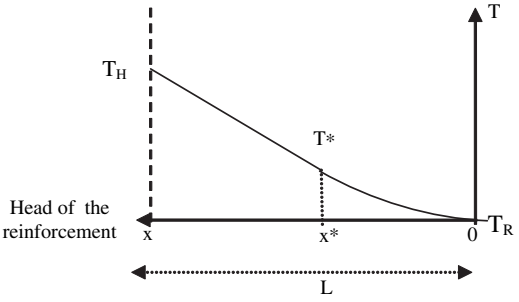

Fig. 18. Tensile-load variation along the reinforcement.

4.6.3. Initial tensile strain threshold (ε_0)

This parameter depends mainly on the initial tension conditions of the strap. Its values cannot thus be generalised. In our modellings, the order of magnitude of ε_0 varies between 0.3% and 0.45% in the case of one synthetic strap, between 0.3% and 0.6% in the case of two synthetic straps and equal to zero in the case of the metallic strip.

5. Conclusion

The experimental part of this study, which concerns the laboratory pull-out tests, enabled us to analyse and to define the parameters influencing the interface behaviour of the synthetic and metallic strips with sand under various confinement stress levels.

The behaviour of these two reinforcement types (metallic and synthetic) is very different:

- The behaviour of these two reinforcement types (metallic and synthetic) is very different:
- The friction mobilisation along the metallic reinforcement is instantaneous for any confinement stress.
- The synthetic strap behaviour is more complex. Tensions as well as displacements are gradually mobilised from the head to the rear of the strap. So, the tail is mobilised after the displacement threshold at the head is reached. This threshold depends mainly on the strap stiffness, the set up conditions of the strap and the confinement stress.

The maximum friction coefficient at the soil/reinforcement interface decreases as the confinement stress increases on the two types of reinforcement (metallic and synthetic). This phenomenon is due to the constrained dilatancy of the ground which leads to the increase in the vertical stress under low confinements.

The tests carried out on synthetic straps show that the use of two parallel, closely spaced, synthetic straps increases the friction parameters at the soil/reinforcement interface. This increase is probably related to an arching effect which is created between the two straps and thus increases the friction area around the inclusions.

Considering the real strip stiffness model as well as the soil/synthetic reinforcement interface friction model of the experimental tests, more realistic modelling methods are determined. Indeed, three modelling approaches have been implemented:

- the first model (M1) considers simple behaviours for the two models (friction and stiffness model), this method adopts an elasto-plastic behaviour of the friction and strip stiffness models. The experimental results show that this method does not concord with the synthetic reinforcement behaviour.
- The second model (M2) considers a more realistic friction model represented by a square root curve and a classical strip stiffness model. It gives a better simulation of the synthetic strap behaviour.
- The third model (M3), in addition to the square root friction model, takes into account the real strip stiffness model. In order to take into account the delay of mobilisation along the strip, an initial deformation ε_0 in the strip stiffness model is used.

Modelling of all tests by the third method (M3) enabled us to simulate accurately the behaviour of synthetic straps under various conditions, validating the new friction and strip stiffness models and finally defining the soil/reinforcement interaction parameters.

The database will allow us to better take into account the phenomenon of soil/reinforcement interaction in structures reinforced by synthetic strips. The models have to be implemented in numerical codes and will permit a better understanding of the behaviour and inherent safety of such MSE walls.

Appendix A

Terzaghi's formula (1943) permits the calculation of the vertical stresses (σ_v) applied along a ground column assuming that stresses are proportional to the arching developed in the ground (Jenck et al., 2005).

$$\sigma_v = \frac{\gamma B_C}{2Ka\tan\phi_R}\left(1-e^{-2Ka\tan\phi_R\frac{He}{B_C}}\right)+(\gamma(H_R-He)+\sigma_0)e^{-2Ka\tan\phi_R\frac{He}{B_C}}$$

The definition and the values of the parameters are reported in Table 6.

Table 6
Parameters used for Terzaghi's formula.

Parameter	Definition	Value
Ka	Coefficient of active pressure. In this case we take Ka = K_0	0.5
B_C (m)	Column width of soil	1.1
H_R (m)	Soil height	1.1
He (m)	Height of equal soil settlement	1.1
σ_v (kPa)	Vertical stress along the column of the soil	–
σ_{v1} (kPa)	Vertical stress at the bottom of the column of soil	–
σ_0 (kPa)	Surcharge	0
φ_R (°)	Friction angle of the soil	38

For a homogeneous settlement: **He = H_R** (Russell and Pierpoint, 1997), hence the vertical stress applied at the bottom of the column (σ_{v1}) can be calculated as following:

$$\sigma_{v1} = \frac{\gamma B_C}{2Ka\tan\phi_R}\left(1-e^{-2Ka\tan\phi_R\frac{He}{B_C}}\right)+\sigma_0 e^{-2Ka\tan\phi_R\frac{He}{B_C}}$$

Appendix B

The analytical development of the first modelling (M1) equation leads to three mobilisation stages of the reinforcement:

1st stage $U_H < U^*$: The strap is in a mobilisation state.

The inclusion is positively directed from the rear R to the head H (Fig. 17). Along an element length *dx*, the elementary tensile-load is given by equation (1).

$$dT(x) = 2bf(x)\sigma_v dx \quad (1)$$

From Fig. 8, we deduce the relation (2).

$$\frac{dT(x)}{dx} = \frac{2bf^*\sigma_v}{U^*}U(x) \quad (2)$$

$$\frac{dU(x)}{dx} = \frac{T(x)}{J} = \varepsilon(x) \quad (3)$$

The local strain $\varepsilon(x)$ at the position *x* is calculated from the inclusion tensile-load model (Fig. 7).

$$\frac{d^2T(x)}{dx^2} = \frac{1}{\rho^2}T(x) \text{ with } \rho = \sqrt{\frac{JU^*}{2bf^*\sigma_v}} \quad (4)$$

The general solution of differential equation (4) leads to equation (5a).

$$T(x) = A\sinh(x/\rho) + B\cosh(x/\rho) \quad (5a)$$

Applying the initial conditions, for $x = 0$, $T = 0$ we obtain $B = 0$ (6b).

$$T(x) = A\sinh(x/\rho) \quad T_H = A\sinh(l/\rho) \text{ hence } A = \frac{T_H}{\sinh(l/\rho)} \quad (5b)$$

At the reinforcement head $x = l$, $T = T_H$; we can write equations (6) and (7).

$$T(x) = T_H \frac{sh(x/\rho)}{sh(l/\rho)} \tag{6}$$

$$U(x) = \frac{\rho T_H}{J} \frac{ch(x/\rho)}{sh(l/\rho)} \tag{7}$$

2nd stage $U_H > U^*$, $U_R < U^*$: In this stage, the reinforcement is divided in two parts (Fig. 18), a part at the head ($x > x^*$) where the friction is completely mobilised and a part at the rear ($x < x^*$), where the friction is in a mobilisation state.

Zone 1. $x > x^*$: T^* and x^* evolve with the evolution of the pull-out load and with displacement at the head, these two variables are determined by the equations (10) and (11).

$$dT(x) = 2bf^*\sigma_v dx \text{ and } \frac{dU(x)}{dx} = \frac{T(x)}{J}$$

$$T(x) = T^* + pf^*\sigma_v\left(x - x^*\right) \tag{8}$$

$$U(x) = U^* + \frac{T^*}{J}\left(x - x^*\right) + \frac{2bf^*\sigma_v}{J}\left(x - x^*\right)^2 \tag{9}$$

$$T^* = \frac{JU^*}{\rho} th\left(x^*/\rho\right) \tag{10}$$

$$\frac{bf^*\sigma_v}{J}\left(l - x^*\right)^2 + \frac{U^*}{\rho}\left(l - x^*\right) th\left(x^*/\rho\right) - \left(U_T - U^*\right) = 0 \tag{11}$$

Zone 2. $x < x^*$: In this zone (see Fig. 18), we can apply the equations developed in the 1st stage, where the reinforcement length would be $l = x^*$ and the head tensile-load $T_H = T^*$.

$$T(x) = T^* \frac{sh(x/\rho)}{sh(x^*/\rho)} = \frac{JU^*}{\rho} \frac{sh(x/\rho)}{ch(x^*/\rho)} \tag{12}$$

$$U(x) = \frac{\rho T^*}{J} \frac{ch(x/\rho)}{sh(x^*/\rho)} = U^* \frac{ch(x/\rho)}{ch(x^*/\rho)} \tag{13}$$

3rd stage $U_H > U^*$, $U_R > U^*$: The strap is entirely released
$dT(x) = 2bf^*\sigma v\, dx$ and $\frac{dU(x)}{dx} = \frac{T(x)}{J}$,
then $T(x) = 2bf^*\sigma v x - C1$, (where C1 is a constant)
for $T = 0$ et $x = 0$:

$$T(x) = 2bf^*\sigma v x \tag{14}$$

then:
$U(x) = \frac{bf^*\sigma v x^2}{J} - C2$ (where C2 is a constant)

for $x = 0$ $U(x) = U_R$

$$U(x) = \frac{bf^*\sigma v x^2}{J} + U_R$$

However, T_H cannot exceed $T_H = 2bf^*\sigma v l$

When U_H is the data:

$$U_H = \frac{bf^*\sigma v l^2}{J} + U_R$$

$$U(x) = U_H - \frac{bf^*\sigma_v}{J}\left(l^2 - x^2\right) \tag{15}$$

References

Abramento, M., Whittle, A.J., June 1995. Analysis of pull-out tests for planar reinforcement in soil. Journal of Geotechnical Engineering, 476–485.

Alfaro, M.C., Miura, N., Bergado, D.T., 1995. Soil geogrid reinforcement interaction by pullout and direct shear tests. Geotechnical Testing Journal GTJODJ 18 (2), 157–167.

Ballegeer, J.P., Wu, J.T.H., 1993. Intrinsic load-deformation properties of Geotextile. Geosynthetic Soil Reinforcement testing procedures. In: Cheng, S.C.J. (Ed.), Proceedings of a symposium held in San-Antonio, Texas, USA. ASTM Special Technical Publication 1190, pp. 16–31.

Bourdeau, Y., Kastner, R., Bollo-Kamara, N., Bahloul, F., 1990. Comportement en ancrage d'un géosynthétique enfoui dans un matériau bidimensionnel. 5ème colloque Franco-Polonais de Mécanique des sols Appliquée, 4–7 septembre.

Cambefort, 1964. Essai sur le comportement en terrain homogène des pieux isolés et des groupes de pieux. Annales I.T.B.T.P., n° 204, Décembre 1964.

Flavigny, E., Desrues, J., Palayer, B., 1990. Le Sable d'Hostun RF, note technique. Revue Française de Géotechnique 53, 67–69.

Frank, R., Zhao, S.R., 1982. Estimation par les paramètres pressiométriques de l'enfoncement sous charge axiale de pieux forés dans les sols fins. Bulletin de liaison des Laboratoires des Ponts et Chaussées 119, 17–24.

Gay, O., 2000. Modélisation physique et numérique de l'action d'un glissement lent sur des fondations d'ouvrages d'art. Thèse de doctorat en Mécanique, Laboratoire 3S, Grenoble 1.

Gurung, N., Iwao, Y., Madhav, M.R., 1999. Pullout test model for extensible reinforcement. International Journal for Numerical and Analytical Methods in Geomechanics 23, 1337–1348.

Jenck, O., Dias, D., Kastner, R., 2005. Soft ground improvement by vertical rigid piles two-dimensional physical modeling and comparison with current design methods. Soils and Foundations 45 (6), 15–30.

Khedkar, M.S., Mandal, J.N., 2009. Pullout behaviour of cellular reinforcements. Geotextiles and Geomembranes 27 (4), 262–271.

Koerner, R.M., Soong, T.Y., 2001. Geosynthetic reinforced segmental retaining walls. Geotextiles and Geomembranes 19 (6), 359–386.

Leshchinsky, D., 2009. On global equilibrium in design of geosynthetic reinforced walls. J. Geotech. and Geoenvir. Engrg 135, 309.

Ling, H.I., Liu, H., Mohri, Y., 2005. Parametric studies on the behavior of reinforced soil retaining walls under earthquake loading. Journal of Engineering Mechanics 131, 1056.

Ling, H.I., Wu, J.T.H., Tatsuoka, F., 1992. Short-term strength and deformation characteristics of Geotextiles under typical operational conditions. Geotextiles and Geomembranes 11 (2), 185–219.

Norme française NF P 94-270, 2009. « Renforcement des sols. Ouvrages en sol rapporté renforcé par armatures ou nappes extensibles et souples. Dimensionnement. ». Editions AFNOR.

Palmeira, E.M., 2009. Soil–geosynthetic interaction: modelling and analysis. Geotextiles and Geomembranes 27 (5), 386–390.

Palmeira, E.M., Milligan, G.W.E., 1989. Scale and other factors affecting the results of pull-out tests of grids buried in sand. Géotechnique 39 (3), 511–524.

Racana, N., Grédiac, M., Gourvès, R., 2003. Pull-out response of corrugated geotextile strips. Geotextiles and Geomembranes 21, 265–288.

Russell, D., Pierpoint, N., 1997. An assessment of design methods for piled embankments. Ground Engineering 30 (10), 39–44.

Schlosser, F., Elias, V., 1978. Friction in Reinforced Earth, A.S.C.E. Convention Pittsburgh, April 24–28.

Schlosser, F., Guilloux, A., 1981. Le frottement dans le renforcement des sols. Revue française de géotechnique 16, 65–77.

Segrestin, P., Bastick, M., 1996. Comparative Study and Measurement of the Pull-out Capacity of Extensible and Inextensible Reinforcements. In: Ochiai (Ed.), Earth Reinforcement. Balkema, Rotterdame, pp. 81–87.

Sieira, A.C.C.F., Gerscovich, D.M.S., Sayão, A.S.F.J., 2009. Displacement and load transfer mechanisms of geogrids under pullout condition. Geotextiles and Geomembranes 27 (4), 241–253.

Sobhi, S., Wu, J.T.H., 1996. An interface pullout formula for extensible sheet reinforcement. Geosynthetics International Journal 3 (5), 565–582.

Su, L.J., Chan, T.C.F., Yin, J.H., Shiu, Y.K., Chiu, S.L., 2008. Influence of Overburden Pressure on Soil–Nail Pullout: Resistance in a Compacted Fill. Journal of Geotechnical and Geoenvironmental. Engineering 134, 1339.

Won, M.S., Kim, Y.S., 2007. Internal deformation behavior of geosynthetic-reinforced soil walls. Geotextiles and Geomembranes 25 (1), 10–22.

Wu, J.T.H., 1991. Measuring inherent load-extension properties of Geotextile for design of reinforced structures. Geotechnical testing journal 14 (2), 157–165.

Yoo, C., Kim, S.B., 2008. Performance of a two-tier geosynthetic reinforced segmental retaining wall under a surcharge load: Full-scale load test and 3D finite element analysis. Geotextiles and Geomembranes 26 (6), 460–472.

Yoo, C., Jung, H.Y., 2006. Case History of Geosynthetic Reinforced Segmental Retaining Wall Failure. Journal of Geotechnical and Geoenvironmental. Engineering 132, 1538.